P1.5 Impact of Wind derived from Satellite on Ongoing Japanese long-term Reanalysis project (JRA-25)

Ryo Oyama*, Masami Sakamoto, Masami Tokuno, Nozomu Ohkawara, Shinya Kobayashi, Takanori Matsumoto, Hiroshi Koide, Kazutoshi Onogi, Tomoaki Ose

Japan Meteorological Agency, Tokyo, Japan

1. Introduction

The Japan 25-year reanalysis referred to as JRA-25 constitutes a consistent set of global weather analyses for the years 1979 to 2004, which is under a collaboration project of Japan Meteorological Agency (JMA) and Central Research Institute of Electric Power Industry (CRIEPI). The primary purpose of JRA-25 is to offer the reanalysis data set and consistent real-time objective analysis. This year is the last year of this project. At present, the evaluation and utilization to investigate the past climate and meteorological events are mainly promoted by JRA-25 evaluation group.

It is of interest to study how satellite wind data performed together with all other types of data in assimilation systems. Satellite wind data are estimated by identifying and localizing the pattern ("tracer") in successive geostationary satellites images, that is, Atmospheric Motion Vector (AMV) or Cloud Motion Wind (CMW). The others are derived from the polar orbital satellite measurements: scatterometer of QuikSCAT, and IR image of MODIS.

As CMW/AMV data have been generally provided since 1979 in which GARP project was started, they had already used to assimilate in the past re-analysis projects. Kallberg and Uppala (1999) investigated the impacts of SATOB derived from METEOSAT and GOES, and also showed the statistical characteristics of every geostationary satellite winds and overall data in ERA-15 (ECMWF 15 year reanalysis) project.

*Corresponding author: Ryo Oyama, Analysis Division of Meteorological Satellite Center, Japan Meteorological Agency, 3-235 Nakakiyoto Kiyose-shi, Tokyo, 204-0012; e-mail: oyama@met.kishou.go.jp.

Impacts of CMW/AMV on other assimilation systems were also investigated by past researches (Tomassini, 1999; Gupta, et al, 2002; Bormann et al).

In this paper, we noticed the impact and importance of CMW/AMV on JRA-25, which might be used in large numbers during all period. We report the impacts of CMW/AMV in each atmospheric layer on JRA-25 wind field and other physical values. In addition, we also show the characteristics of GMS-AMV reprocessed by Meteorological Satellite Center (MSC) for JRA-25. The data is one of the major improvements not included in other re-analyses.

2. Assimilation methods of CMW/AMV in JRA-25

JRA-25's main characteristics are shown below:

1) Model resolution and Analysis method

Vertical Resolution is 40 layers with the top level at 0.4 hPa, horizontal spectral triangular-truncation at total wave number 106 (T106; equivalent to about 110km grid size). Assimilation method is 3D-VAR, which had been adopted in JMA's operational system from September 26 2001 to February 16 2005.

2) Observation data used in JRA-25

The data used to assimilate in JRA-25 are conventional data: SYNOP, TEMP, PILOT, AIREP, CMW/AMV and so forth, and satellite remote sensing data: sounder data of TOVS and ATOVS, and sea temperature and sea ice data from SSM/I. CMW/AMV data are used throughout the entire period of JRA-25. METEOSAT wind products between 1982 and 1988 were reproduced by the new algorithm using the recalibrated images of METEOSAT-2 and 3 (Van de berg, L., et al, 2001). Moreover, these have been made as BUFR including QI information since

September 7 1998.

AMV derived from GMS were reproduced by a MSC new operational algorithm (Kumabe, 2004) in the period between April 1987 and May 2003.

3. Characteristics of MSC reprocessed AMV

MSC of JMA processed High-density Atmospheric Motion Vector (AMV) from GMS-3 to GMS-5 for the period of 1987 to 2003. These are processed on the basis of MSC operational AMV extraction method (Kumabe, 2004). Because of defect in the production, the periods when JRA-25 used those products are limited to March 1987 - December 1993, and January 1997 - May 2003. Main features of GMS AMV are,

a) Relatively high Quality Indicators (QI)

For each vector of GMS AMV, QI is assigned with the same procedure as the EUMETSAT operational AMV processing (Holmlund, 1997). However, the wind vector extraction procedure itself is MSC in-house, and differs from the EUMETSAT's. Accordingly, for each wind computational method, the distribution of QI is considerably different from EUMETSATs, which have rather constant counts in each division of ranks for all kinds of vectors. IR high winds and WV winds of GMS have peaks on their division of QI magnitude from 81 to 85, IR low and VIS winds tended to have their peak on higher QI divisions. (**Fig. 1-1**)

b) Sparse Mid-level IR Winds

Essentially, IR wind vector is processed with two distinctive measures, which are referred as the IR high winds derived from clouds of semi-transparency and the IR low winds derived from opaque clouds generally. At the first step in the MSC IR wind processing technique, IR images are distinguished into 2 levels: above 500hPa and below 850hPa. Consequently, IR vectors at between 500 and 850hPa are rarely produced as shown in **Figure 1-2**.

c) Only GMS-5 has WV winds

For the first time of the long records of GMS series observation, GMS-5 launched in Mar 18 in 1995 boarded the imager with WV absorption channel, and it came into operation on June 13 in 1995. WV derived winds were also archived from that day to May 2003, when GMS-5 finished its operation.

d) Narrower Production Area

GMS AMV were processed over the round shaped area bounded 50S and 50N, 90E and 170W (see **Fig. 1-3**), which was narrower than ones of satellite derived winds of the other operational centers.

The high-density winds with quality indicators surely permit free choices of the utilization for NWP centers and reanalysis organizations. But it requires more sophisticated measures for selection, thinning, and evaluation of bias. Because AMVs tend to have inhomogeneous spatial distribution, especially ones with higher QI incline to concentrate narrow areas and are found to have the similar behavior in the small area, which can affect substantially data-assimilation products with the variational techniques

4. Experiments to investigate the impact of CMW and AMV

4.1 Outline of Experiments

To investigate impacts of CMW/AMV on JRA-25, in addition to CTRL experiment which includes all CMW/AMW of all satellites, we tried two ones: 1) Experiment without the upper (above 400 hPa level) and 2) without the lower layer (below 700 hPa level). We refer to these as "TEST1" and "TEST2" respectively (see **Table 1)**. The experiment period is between 00UTC July 1 2003 and 18UTC July 31 2003. In this period, CMW/AMV derived from IR, VS, and WV images of METEOSAT-5 and 7, and GOES-9, 10, and 12 are used. Here, CMW/AMV from GOES-9 is MSC's present improved product explained above.

Table1: Configurations of TEST1, TEST2, and CTRL

	TEST1	TEST2	CTRL
Upper Layer CMW/AMV (Above 400hPa level)	None	Used	Used
Middle Layer CMW/AMV (700hPa to 400hPa)	Used	Used	Used
Lower Layer CMW/AMV (Below 700hPa level)	Used	None	Used

4.2 Analysis Impacts on CMW/AMV

We show the horizontal distribution of the wind difference (Increment) between the analysis and the first guess of CTRL in **Figure 2**. Large Increments are found in some part of Antarctic. One of the reasons is conventional data are sparse in the south hemisphere. In upper layer (300 hPa), Increments are larger in Indian Ocean, east coast of North America and southwestern Atlantic Ocean. In the lower layer (850 hPa), they are distinctly larger over Indian Ocean, Tibet Plateau, western America and west of South America. These facts suggest that these regions and levels should be sensitive to the assimilated observational data.

4.2.1 Impact of Upper layer CMW/AMV

Figure 3 and **Figure 4** show the monthly averaged difference of zonal wind analyses and forecasted precipitation rate between CTRL and TEST1. We can find out there are some interesting impacts on them, especially, on precipitation rate in the tropics, its feature might closely connect to seasonal oscillation of tropical precipitation. The results of investigations are shown below in detail.

(a) Tropical Indian Ocean (30S-30N and 25E-85E: A-1)

At 400-200 hPa levels, the difference of dominant easterly wind speed attains to a speed of 5m/sec or more over Equator-10N and around 55E with use of the upper layer CMW/AMV (see **Fig. 5**). This result well corresponds to the past research by Tomassini et al (1999) and Bormann et al. Distinct negative Increments of winds are found there (see **Fig. 2**).

In addition, we can find out the impacts on spatial and quantity distribution of precipitation connected to both horizontal circulation and geopotential height fields. According to the vertical cross section of the rotation at 55E of them (as shown in **Fig. 6**), the use of upper layer CMW/AMV caused the decrease of the rotation at higher than 550 hPa level. As the divergence at 600-400 hPa levels is weakened over Equator-10N while intensified at 400-250 hPa levels, a maximum peak of geopotential height is produced at around 400 hPa level. By these impacts, convection is refrained at 500-300 hPa levels (see **Fig. 7**). The precipitation rate of CTRL is less than TEST1 by 1.5 to 2.0 mm/hour in the region (shown by blue oval in **Fig. 7(b)**), while that of CTRL is larger than TEST1 around there (shown by red oval in **Fig. 7(b)**). In addition, the temperature of CTRL is less than TEST1 by 0.3 degrees or more at 600-500 hPa levels, and the specific humidity of CTRL is larger than TEST1 only at 700-450 hPa levels. These might suggest a heating caused by the convection should be restricted to only under about 400 hPa level.

(b) Southern middle and high latitudes of Indian Ocean (80S-20S and 10E-70E: A-2)

In this region, dominant westerly zonal winds at 400-200 hPa levels are weakened by 1.5 to 2.0 m/s around 45S with use of upper layer CMW/AMV (**Fig. 8-1**). On the other hand, the most distinct feature is appears in geopotential height and air temperature fields in spite of the small modification of wind field. The symmetric feature with respect to 45S in the vertical cross section at 40E of temperature and geopotential height is interesting (**Fig. 8-2**).

(c) Western middle and south of Africa (45S-15N and 10W-50E: A-3)

It is found that dominant easterlies at 600-300 hPa levels are intensified by 0.5-2.5 m/s over 10S-10N (see **Fig. 9)** when upper layer CMW/AMV data are used and negative Increments are found there (see **Fig. 2**).

According to relative humidity, the reduction over 10S to 5N and enlargement over the north and south to there in middle and lower layers well correspond to the divergence and convergence zones there respectively (as not shown here). Such modification of middle and lower wind fields is one of the noticeable

impacts in the region, which might suggest the relation to African topography.

(d) Tropical eastern Pacific Ocean (30S-30N and 150W-90W: A-4)

Upper layer CMW/AMV intensified dominant easterlies by 1-1.5 m/s at 500-400 hPa levels (see **Fig. 10-1** and **10-2**). Here, it is noticeable that large Increments of CTRL is hardly distributed in the level and region. This fact might suggest that upper layer CMW/AMV should well contribute to JRA-25 wind field by the difference of wind between CTRL and TEST1. And, this result partly shows the characteristic of the CMW/AMV derived from GOES-10, which are corrected by the result of numerical model in NESDIS.

4.2.2 Impact of Lower layer CMW/AMV

Figure11 shows the difference of the analyses of physical values between CTRL and TEST2. By and large, lower layer CMW/AMV data tend to modify horizontal circulation field in lower and middle layer. We show the results on every impact below.

(a) Tropical eastern Pacific Ocean (30S-30N and 120W-60W : B-1)

Figure 12-1 shows that dominant easterlies below 400 hPa level are weakened over 5S to 5N, and intensified over 20S to 5S, when lower layer CMW/AMV are used. As the result, anti-cyclonic circulation in lower layer is intensified over 10S to Equator accompanying with the intensification of the lower layer convergence over Equator to 10N (see **Fig. 12-2**). This convergence intensification results in the increase of the monthly averaged precipitation rate there as shown in **Figure 12-3**.

(b)Tropical Indian Ocean (30S-30N and 25E-85E : B-2)

At 850-400 hPa levels, dominant westerly winds around 5N are intensified, and easterlies over 20S to Equator are intensified when lower layer CMW/AMV are used as shown in **Figure 13-2**. As the results, anti-cyclonic circulation at 850-400 hPa levels over 5S to 5N is intensified (see **Fig. 13-1**). Although such reduction of the precipitation over Equator to 5N as A-1 of TEST1 is confirmed, its change is smaller (see **Fig. 13-3**).

(c) Northeast Pacific Ocean (Equator-60N and 160W-100W : B-3)

Below 600 hPa level, cyclonic circulation is intensified over 25N to 35N and at around 125W and anti-cyclonic circulation is intensified over 35N to 45N and at around 135W when lower CMW/AMV are used (see **Fig. 14-1** and **14-2 (a)**). A heating over 35N to 45N and a cooling over 25N to 35N are characteristic in the lower layer (see **Fig. 14-2 (b)**). In spite of these impacts on temperature, the impact on specific humidity is small. It might be one of the reasons that the water vapor is smaller relative to that in the tropics.

5. Statistical feature of impact for each region and satellite

To show the statistical feature of the impacts of the CMW/AMV for each satellite and latitudinal band, we show differences of monthly average and standard deviation (SD) of Increment between CTRL and TEST1 or TEST2 for each satellite, level and region in **Figure 15**.

In northern and southern hemisphere (referred to as NH and SH), when upper layer CMW/AMV data are used, the negative Increment of the upper layer zonal wind become larger of every satellite region, that is, dominant westerly wind are weakened. Especially, such tendency is prominent in winter hemisphere. The difference of SD of Increment is also large there.

In the tropics (referred to as TP), when upper layer CMW/AMV are used, dominant upper layer easterlies are intensified except for at 200-100 hPa levels over METEOSAT-5 coverage, which includes Indian Ocean. Over GOES-12 coverage: North America, Atlantic Ocean and Southeastern Pacific, easterlies at upper layer are weakened. Over GOES-10 coverage: mainly

east Pacific Ocean, modification of wind at upper layer is small.

About the impact of lower layer CMW/AMV, differences of SD of Increment generally decrease at lower layer in TP and SH of each satellite coverage, when the lower layer CMW/AMV data are used. On GOES-12, it is characteristic that SD of CTRL tends to be larger than that of TEST2 at 800-700 hPa in SH and TP. In the upper and middle layers, the impacts due to lower layer CMW/AMV are little for every satellite.

Figure 16 shows the horizontal distribution of monthly SD of D-value of zonal wind in 5×5 degree grids and at 400-300 hPa and 900-800 hPa levels respectively. The results of METEOSAT-5, GOES-10 and 12 are shown, which cover the impact regions in section 4. For every satellite, SD of D-value in upper and lower layers generally tend to be less over the sea.

Within METEOSAT-5 coverage, it found that SD of D-value at both 400-300 hPa and 900-800 hPa levels is larger around A-1 in spite of over the sea. This means that large variability by CMW/AMV data exists there.

Within the coverage of GOES-10 and 12, SD of zonal wind over the sea are generally small, although a little large values (0.5-2.0m/s) exist at the edge of their coverage. These facts suggested that the CMW/AMV from GOES-10 and 12 should be in harmony with the JRA-25, that is, assimilation system using 3D-VAR.

6. Summary

We could confirm the effectiveness and impact of CMW/AMV data on JRA-25 as shown below:

(Upper layer CMW/AMV data)

Upper layer westerly winds over the middle and high latitudes are found to be weakened with the use of upper layer CMW/AMV data, especially distinct in the winter hemisphere.

In the tropical Indian Ocean, dominant upper layer easterlies are intensified by 5m/s or more, when upper layer CMW/AMV are used and negative Increments of zonal wind is found there. The increase of high pressure at around 400 hPa level because of the modification of divergence fields restrains the deep convection. Over western middle and south of Africa, with use of upper layer CMW/AMV, upper layer easterlies are intensified, and the modification of convergence field at middle and lower layers changed the precipitation field. Over southern middle and high latitudes of Indian Ocean, with use of upper layer CMW/AMV, geopotential height and temperature fields are distinctly changed in upper and middle layers while modification of wind field is small there. In tropical eastern Pacific Ocean, dominant easterlies at middle layer are intensified when upper layer CMW/AMV are data used and small Increments of CTRL are found there.

(Lower layer CMW/AMV data)

JRA-25's horizontal circulation fields of the middle and lower layers are generally modified with use of lower layer CMW/AMV data. The precipitation field is changed in the tropics.

When lower layer CMW/AMV are used in the tropical eastern Pacific Ocean, precipitation increases there because the lower layer anti-cyclonic circulation is intensified to make stronger lower layer convergence. In tropical Indian Ocean, precipitation decreases there as well as in the case with use of upper layer CMW/AMV because anti-cyclonic circulation at middle and lower layers is intensified. In northeast Pacific Ocean, a pair of cyclonic and anti-cyclonic circulation is intensified in lower layer without distinct impact on precipitation and specific humidity there.

It is found that use of lower layer CMW/AMV tends to minimize standard deviation of Increment of wind at lower layer.

Acknowledgement

We would thank K. Kato and T. Imai of JMA/MSC for their valuable supports and advices.

References

Bormann, Niels and Thepaut, J.: Impact of Atmospheric Motion Vectors from INDOEX on ECMWF analyses and forecast. *(Met Office HP http://www.metoffice.com/research/interproj/nwpsaf/satwind_report/satwindinfo.html)*.

Gupta M.Das et al. 2002: Impact of high density atmospheric motion vectors in NCMRWF global data assimilation-forecast system. *Proc. of 'Sixth International Winds Workshop', EUMETSAT*, 155-162.

Holmlund, K. 1998: The utilization of statistical properties of satellite-derived atmospheric motion vectors to derive quality indicators, *Weather and Forecasting*, **13**, 1093-1104.

Kållberg, P., and S. Uppala, 1999: Impact of Cloud Motion Winds in the ECMWF ERA15 Reanalysis. *Proc. of 'Fourth International Winds Workshop', EUMETSAT*, 109-116.

Kumabe, R. 2004: Renewal of operational AMV extraction system in JMA. *Proc. of 'Seventh International Winds Workshop', EUMETSAT*, 71-77.

Tomassini, M., Kelly, G. and Saunders, R., 1999: Use and Impact of satellite atmospheric motion winds on ECMWF analysis and forecasts. *Mon.Wea.Rev*., **127**, 971-986.

Van de Berg, L., Gustafsson, J and Yildirim, 2001: Reprocessing of atmospheric motion vectors from METEOSAT image data. *Proc. of 'ERA-40 workshop on Re-analysis'*, 5-9.

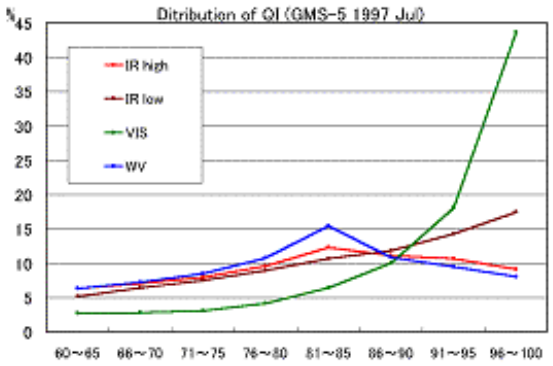

(a) QI distribution of GMS-5

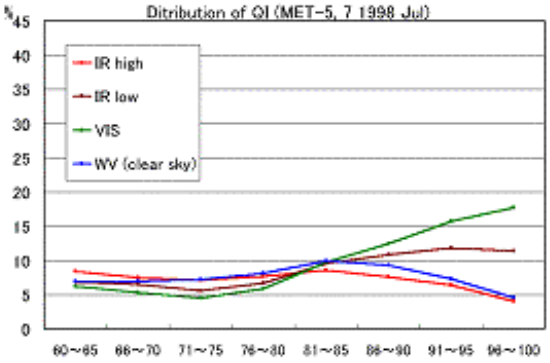

(b) QI distribution of METEOSAT-5 and 7

Figure. 1-1: QI grouped by their magnitude.
(a) GMS-5 in July 1997, (b) METEOSAT-5, 7 in July 1998.
Red: IR high (above 600hPa), Brown: IR lower (below 600hPa), Green: VIS, Blue: WV.

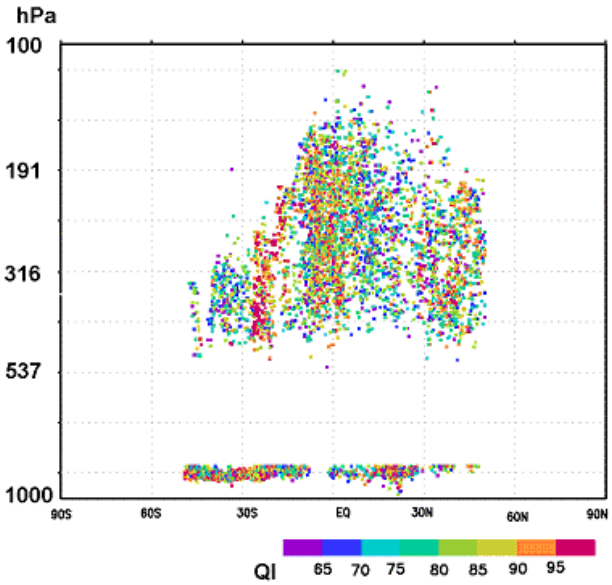

Figure 1-2: Vertical distribution of GMS-5 IR winds with QI magnitude at 12UTC 2 Jul 1997.

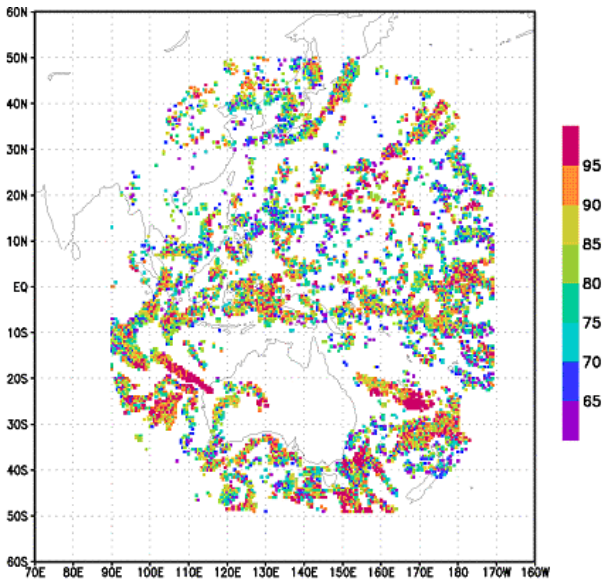

Figure 1-3: Horizontal distribution of GMS-5 IR winds with QI magnitude at 12UTC 2 Jul 1997.

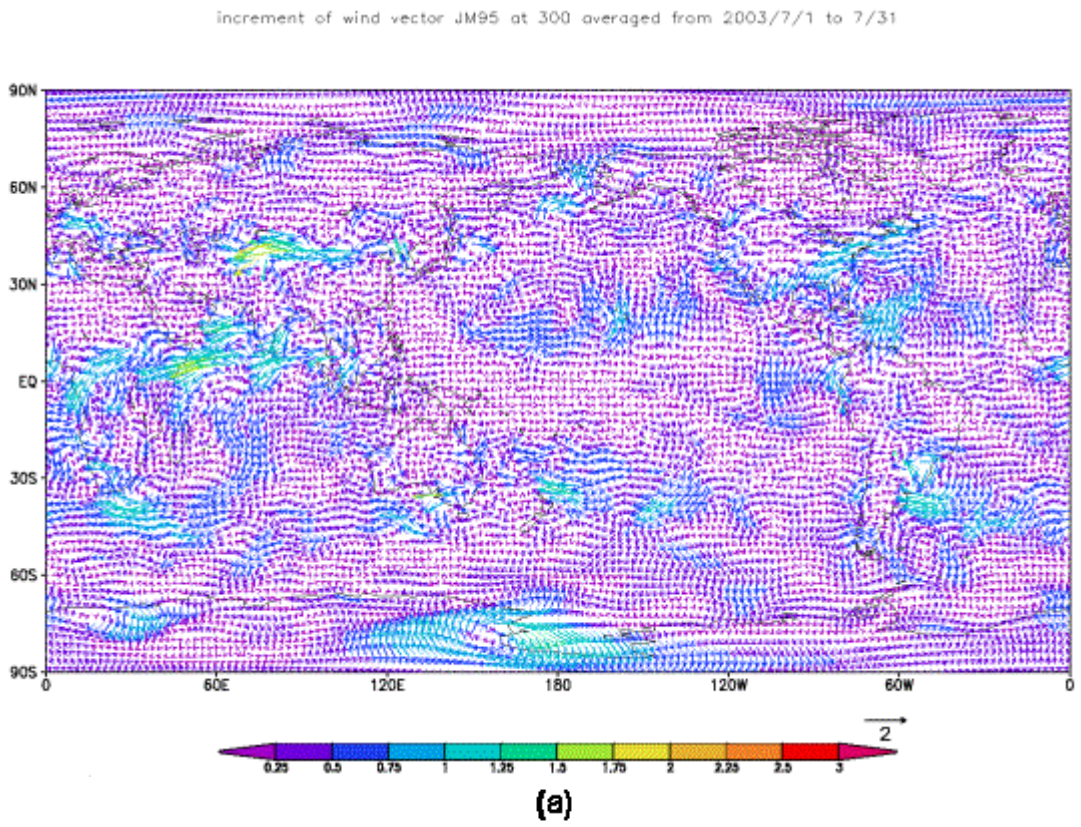

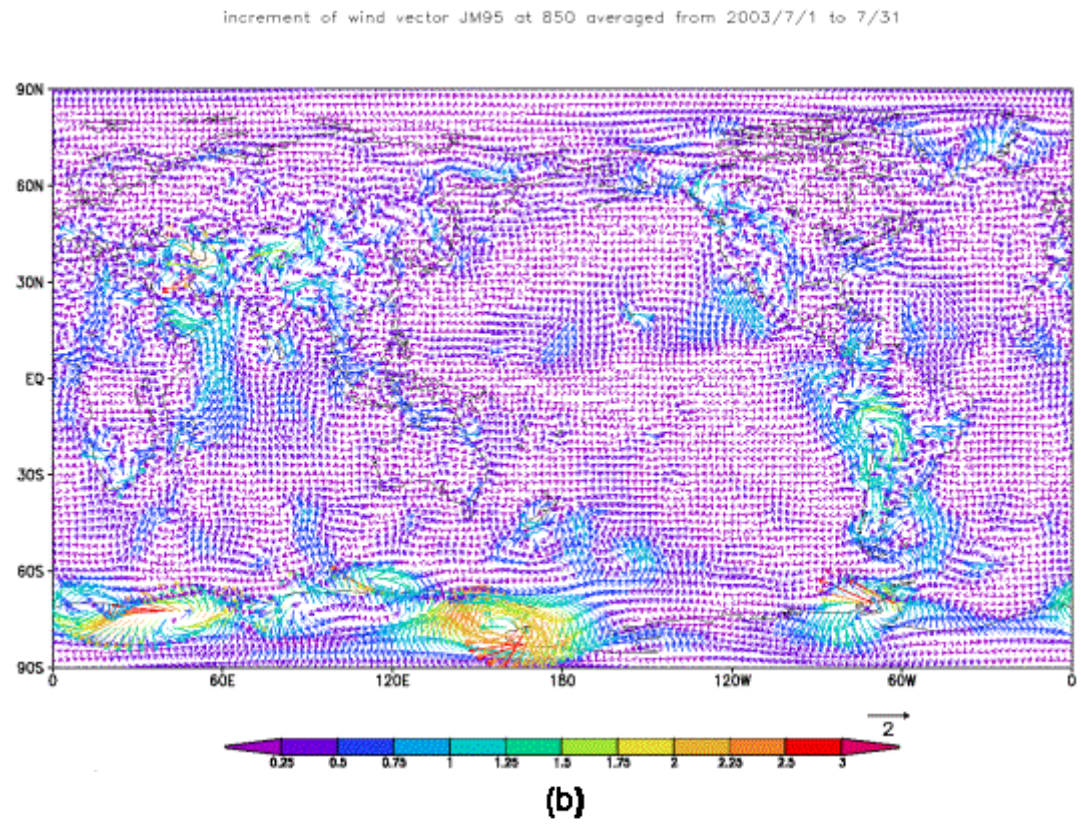

Figure 2: Monthly averaged Increment (Anal – Guess) of CTRL at each level. (a) 300hPa, (b) 850hPa.

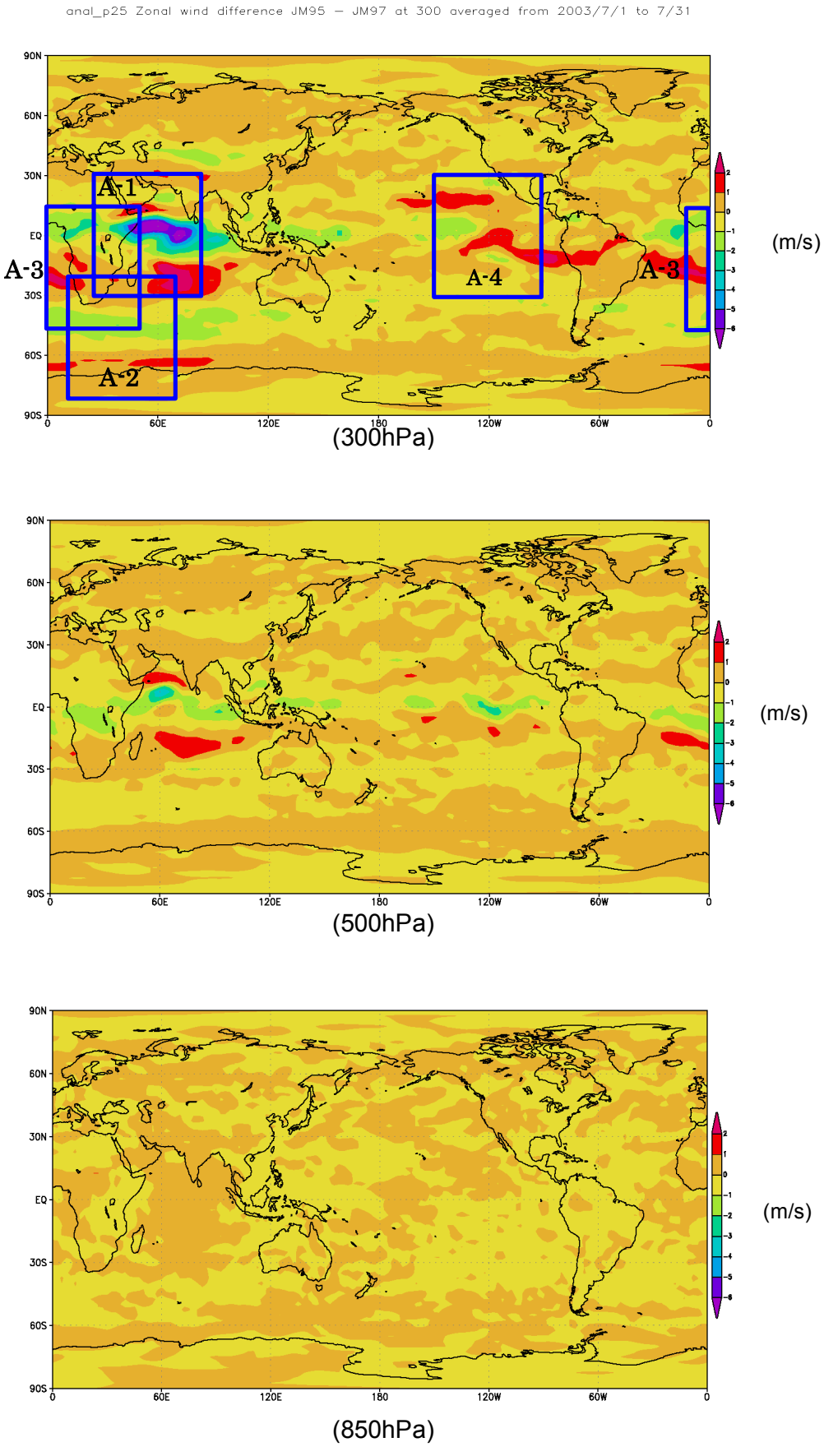

Figure 3: Difference (CTRL-TEST1) of zonal wind analysis at 300, 500 and 850hPa.

(a)

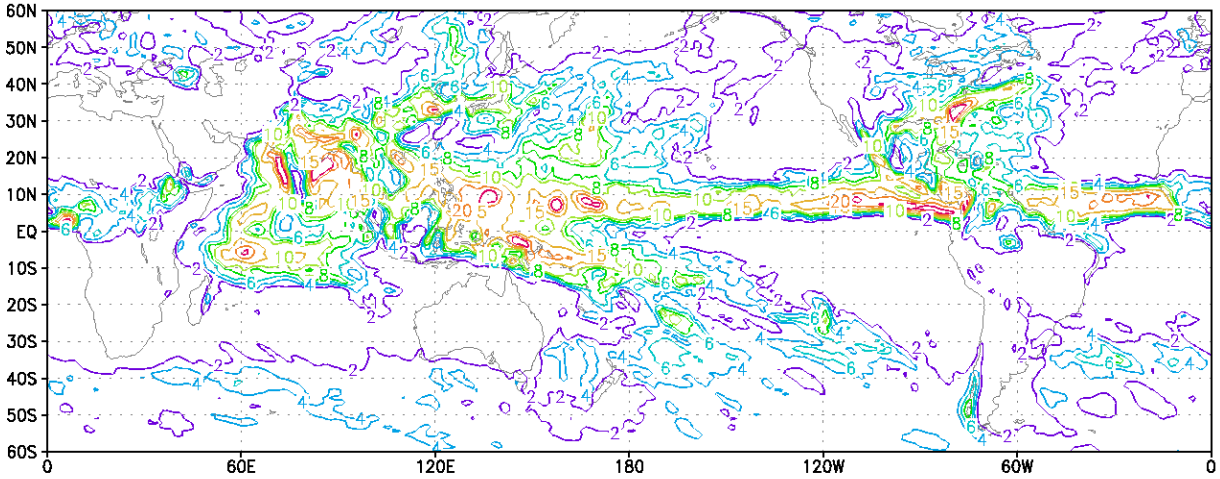

(b)

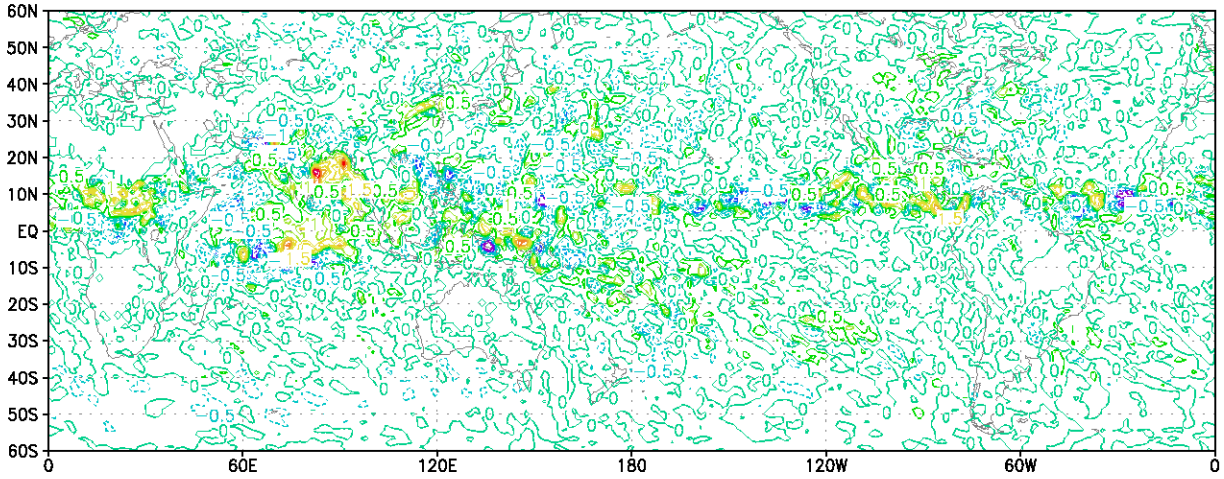

Figure 4: (a) Monthly average of total precipitation rate (mm/hour) of CTRL, (b) Monthly average of difference of total precipitation rate (CTRL-TEST1).

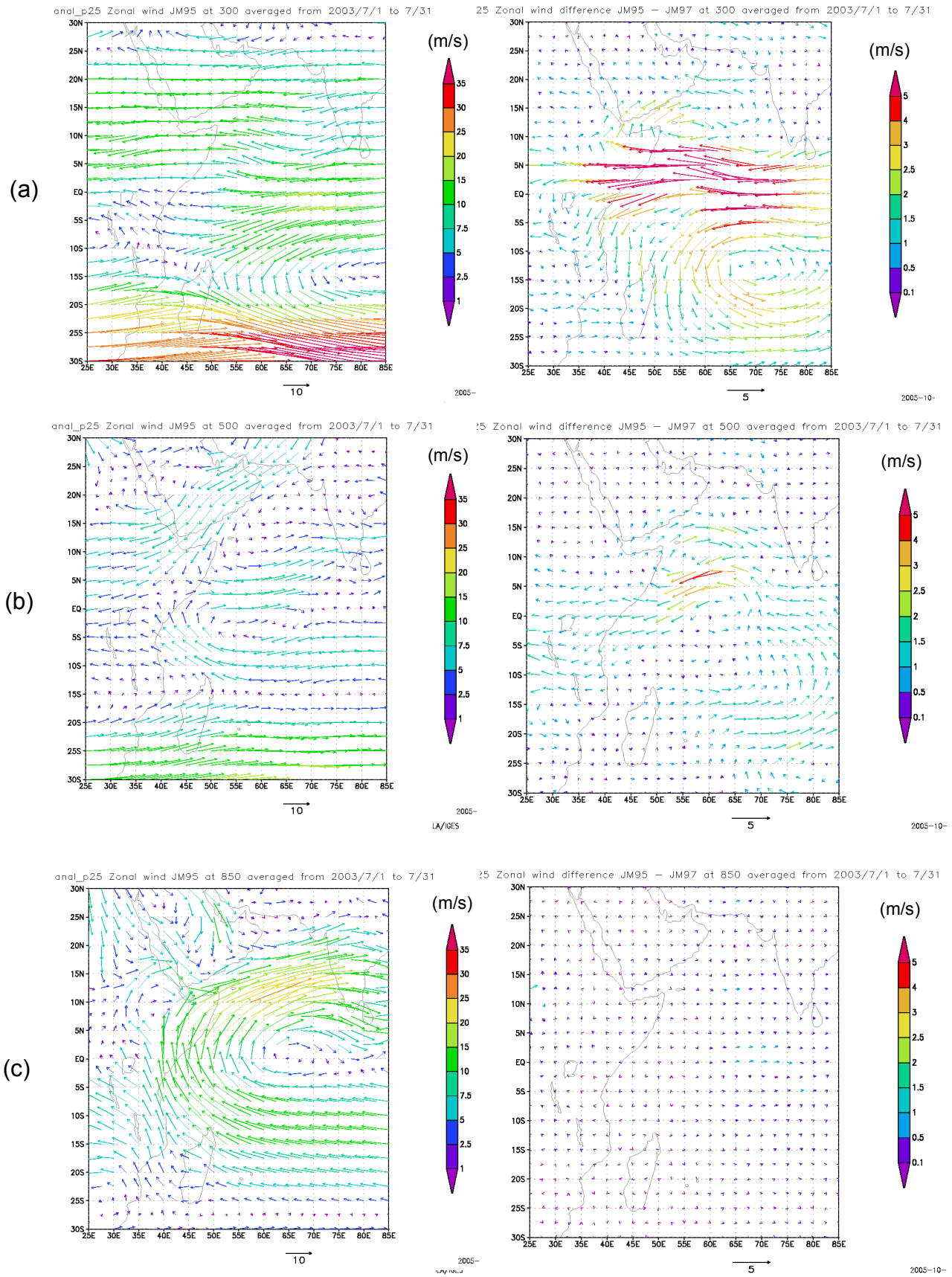

Figure 5: Monthly average of analysis wind (Left), and the difference of monthly averaged analysis wind between CTRL and TEST1 (Right) for region A-1.
(a) 300hPa, (b) 500hPa, (c) 850hPa.

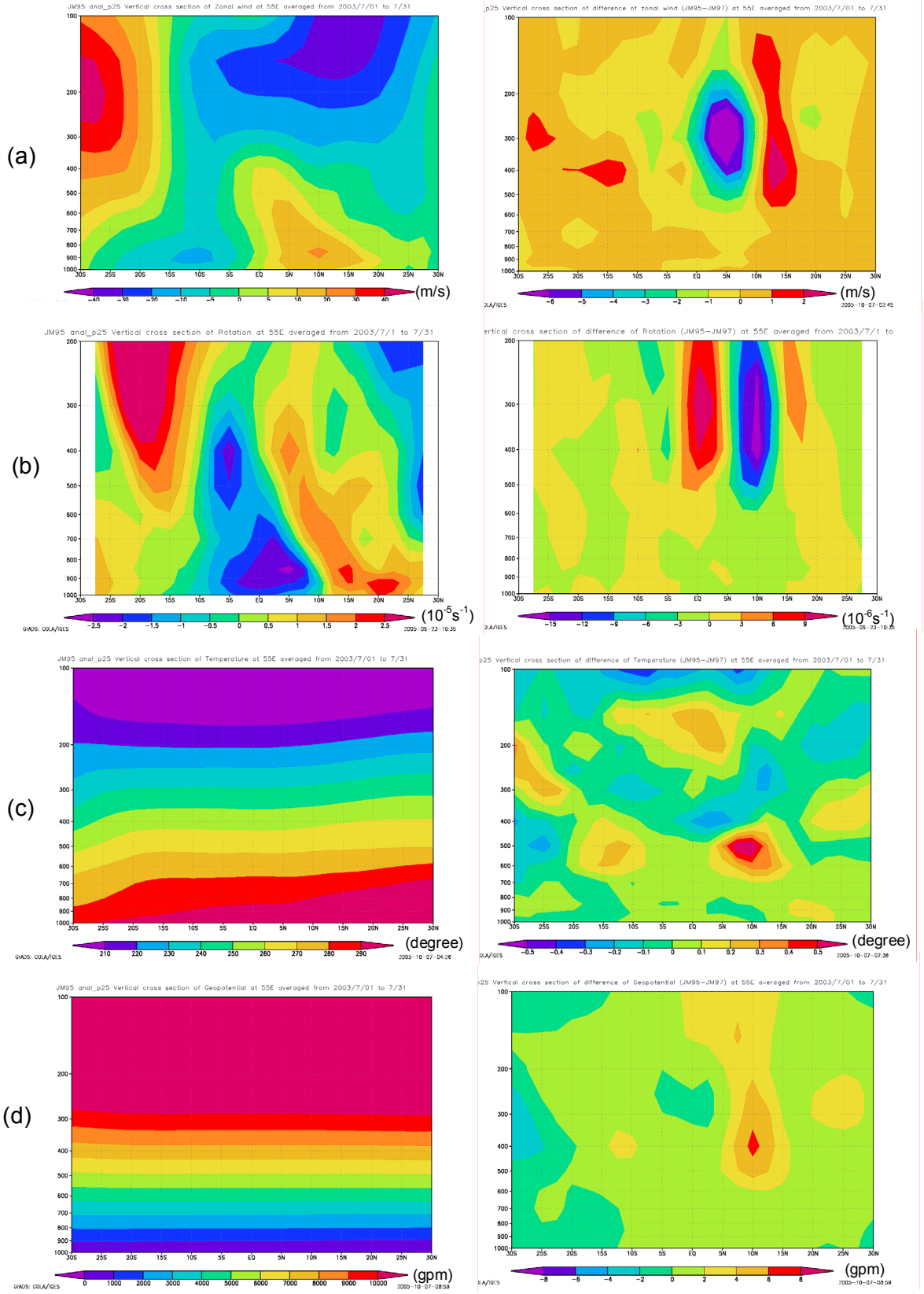

Figure 6: Longitudinal vertical cross-sections of each physical values at 55E (for region A-1). Left: Monthly averaged analysis of CTRL, Right: Difference of analysis (CTRL – TEST1). (a) Zonal wind, (b) Rotation, (c) Temperature, and (d) Geopotential height.

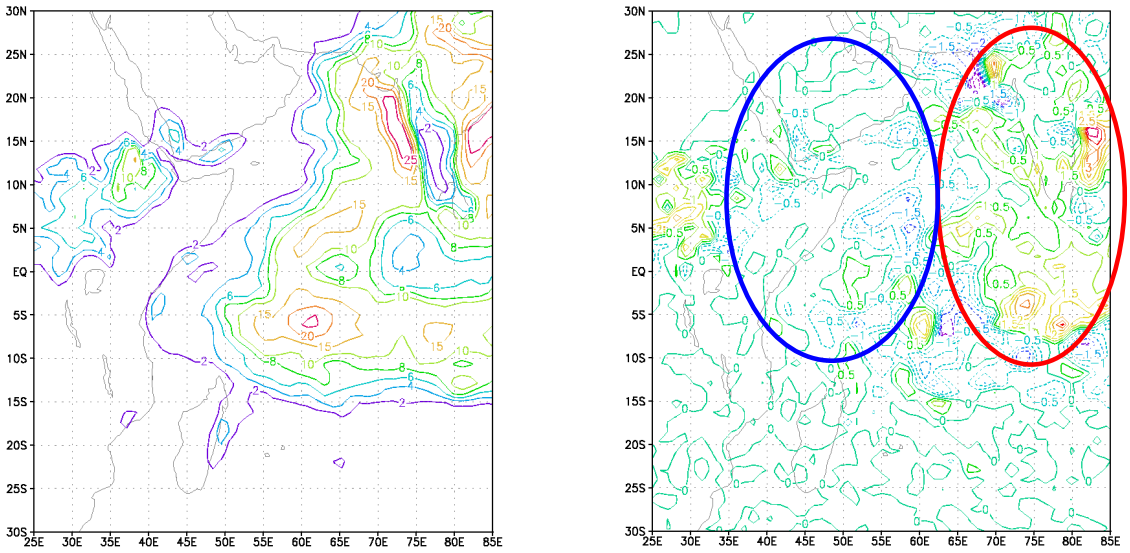

(a) (b)

Figure 7: (a) Monthly averaged precipitation rate (mm/hour) of CTRL, and (b) Difference between CTRL and TEST1 for Region A-1.

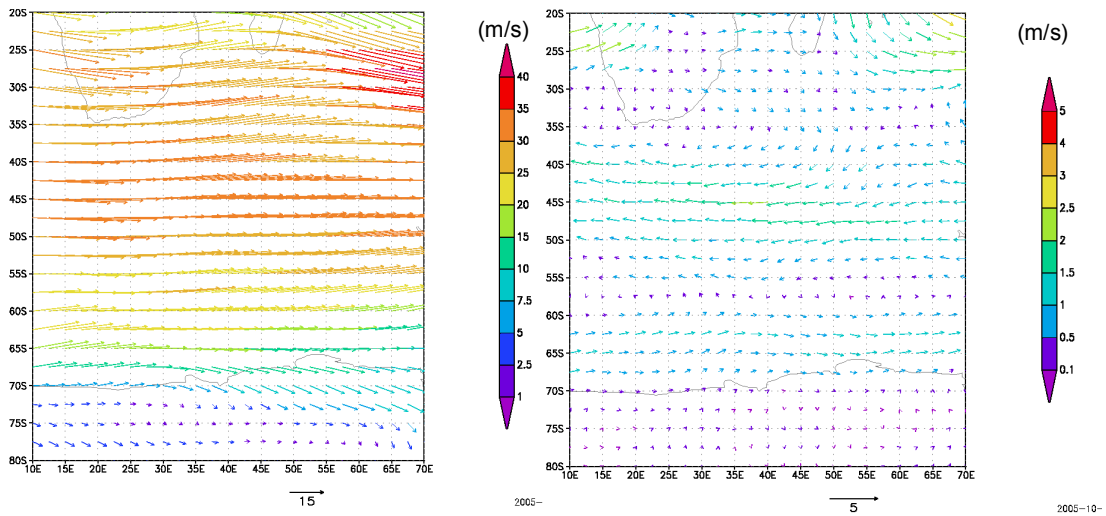

Figure 8-1: Monthly averaged analysis wind at 300hPa of CTRL (Left) and difference of monthly averaged wind at 300hPa between CTRL and TEST1 (Right) for region A-2.

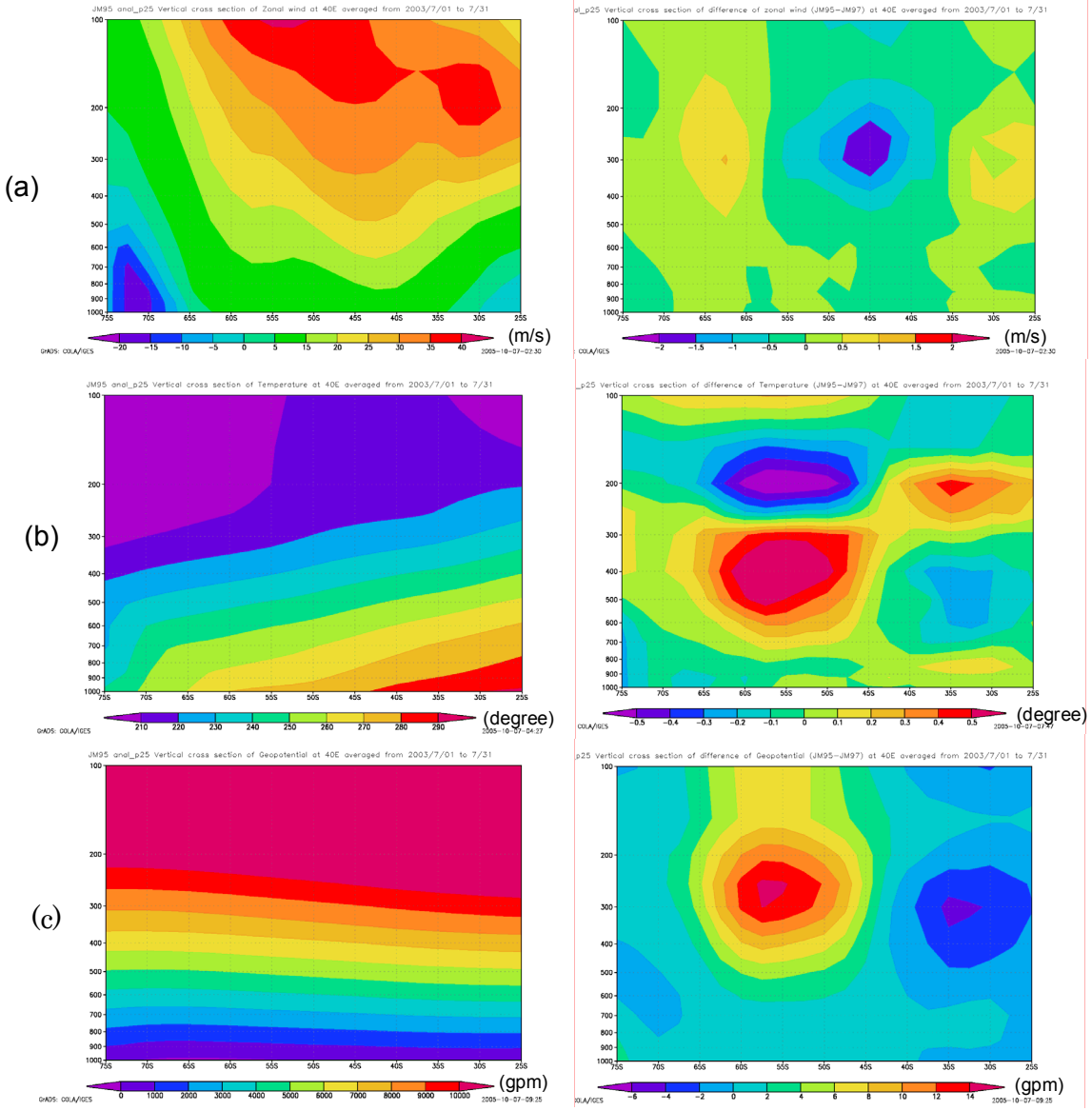

Figure 8-2: Longitudinal vertical cross-sections of each physical values at 40E (for region A-2). Left: Monthly averaged analysis of CTRL, Right: Difference of analysis (CTRL – TEST1). (a) Zonal wind, (b) Temperature, and (c) Geopotential height.

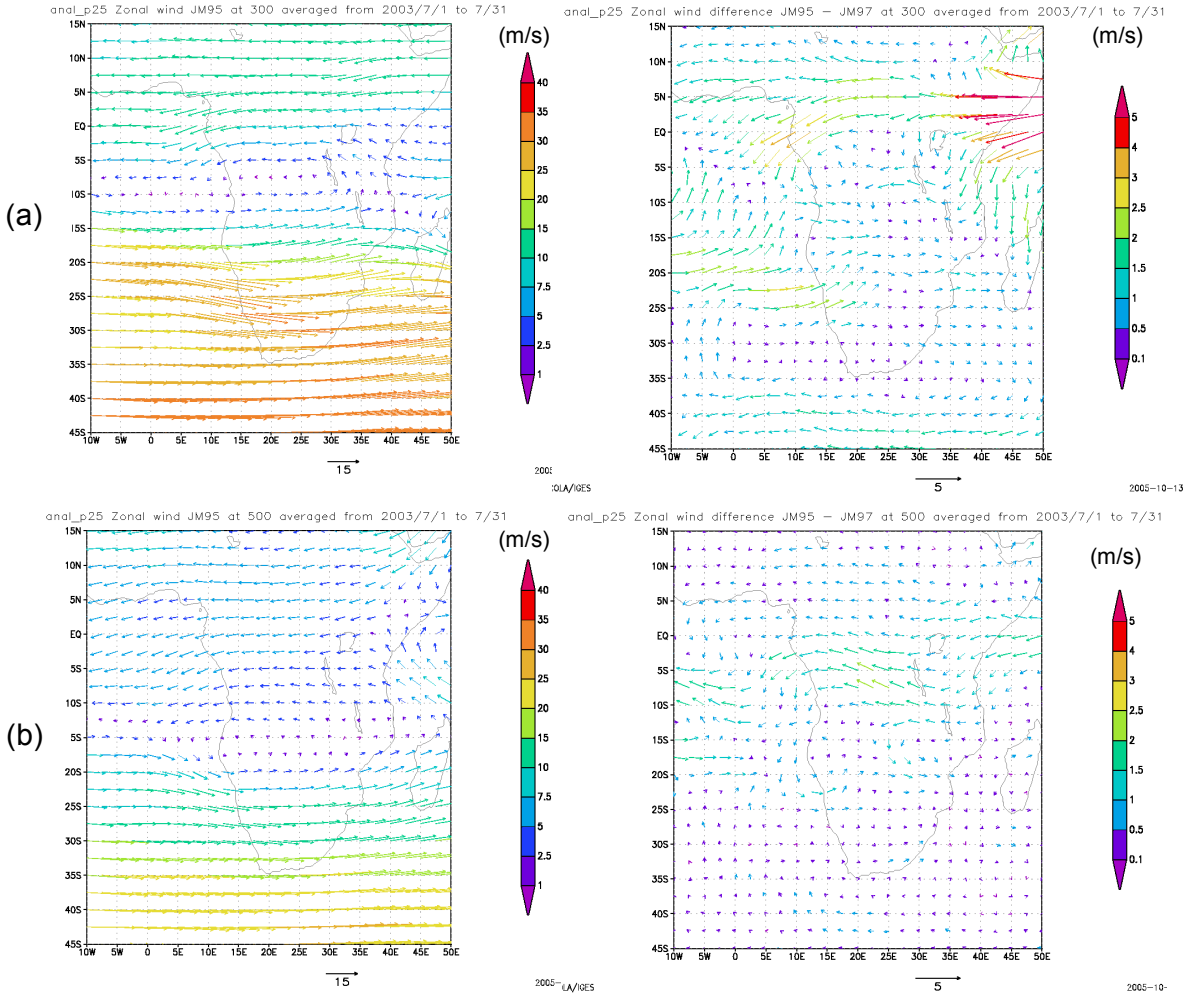

Figure 9-1: Monthly averaged analysis wind of CTRL (Left), and Difference between CTRL and TEST2 (Right) for region A-3. (a) 300hPa, (b) 500hPa.

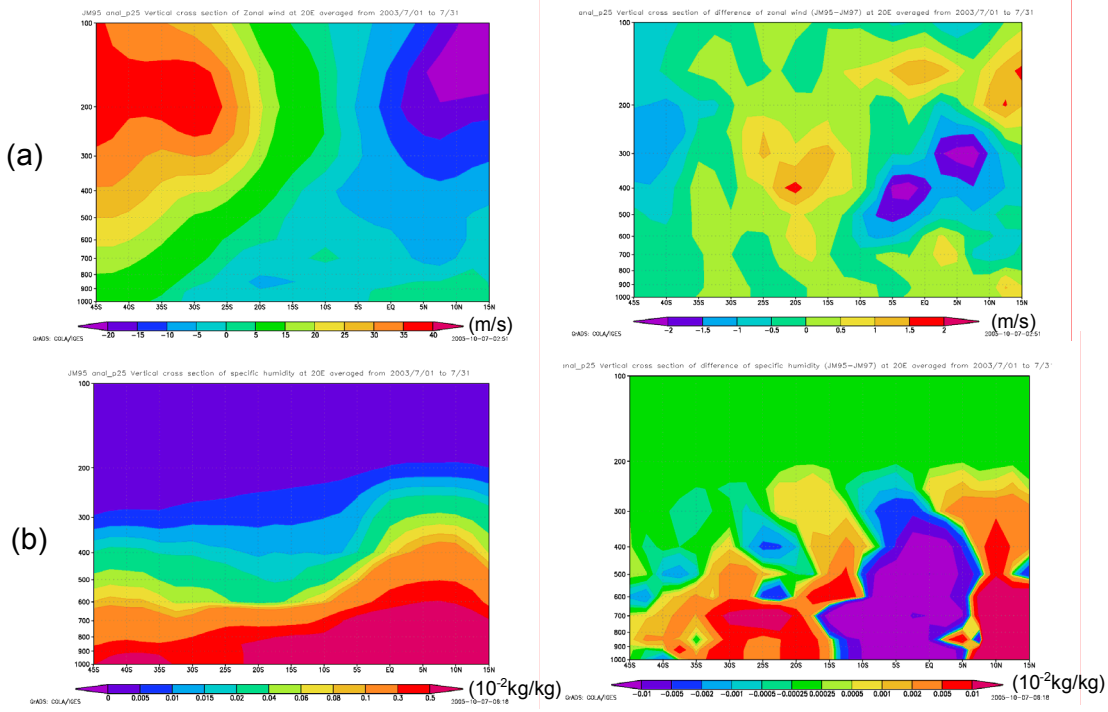

Figure 9-2: Longitudinal vertical cross-sections of each physical elements at 20E (for region A-3). Left: Monthly averaged analysis of CTRL, Right: Difference of analysis (CTRL – TEST1). (a) Zonal wind, (b) Specific humidity.

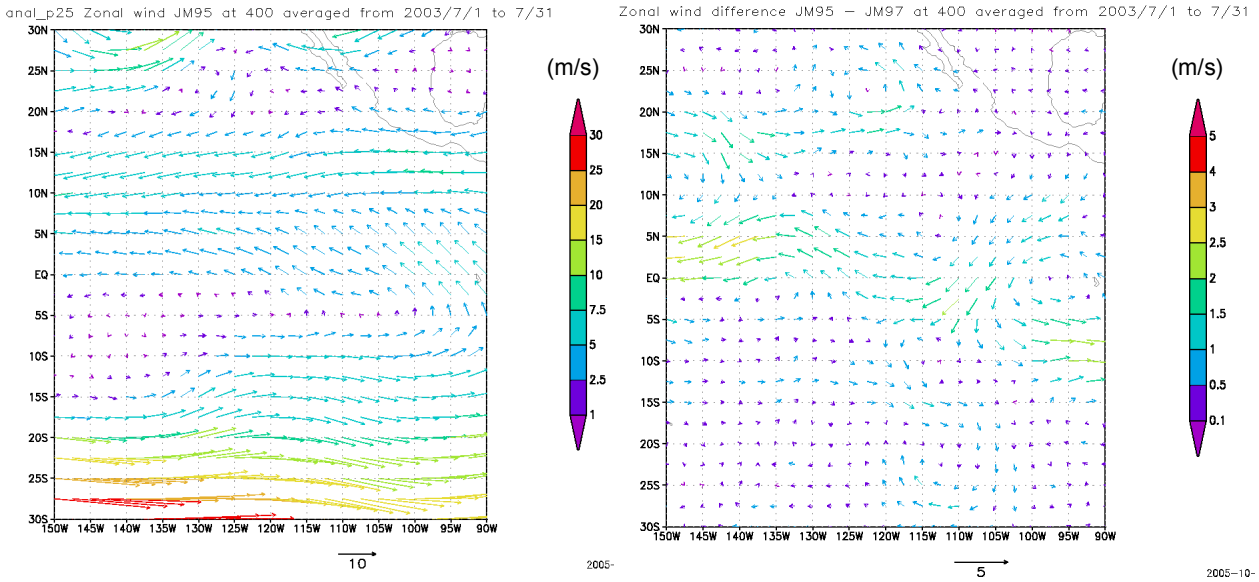

Figure 10-1: Monthly averaged analysis wind at 400hPa of CTRL (Left) and difference of analysis wind at 400hPa between CTRL and TEST1 (Right) for region A-4.

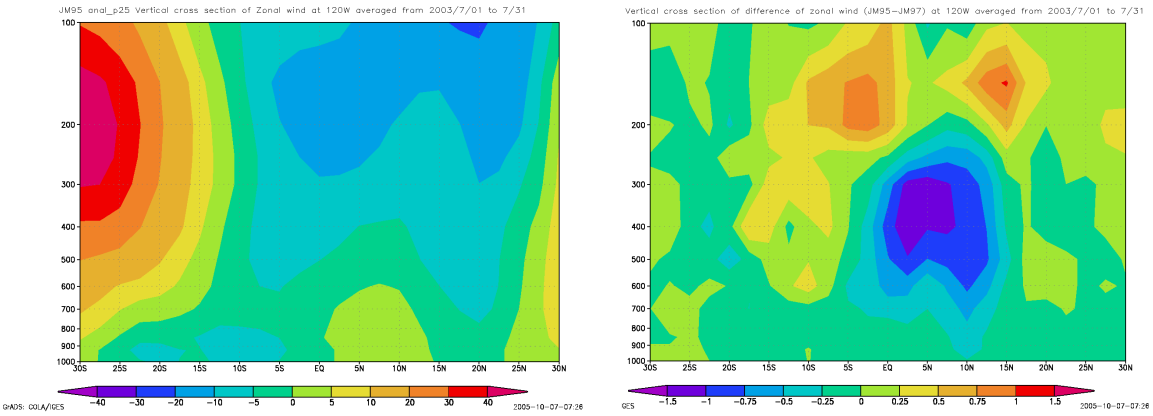

Figure 10-2: Longitudinal vertical cross-sections of zonal wind (m/s) at 120W (for region A-4).
Left: Monthly averaged analysis of CTRL, Right: Difference of analysis (CTRL – TEST1).

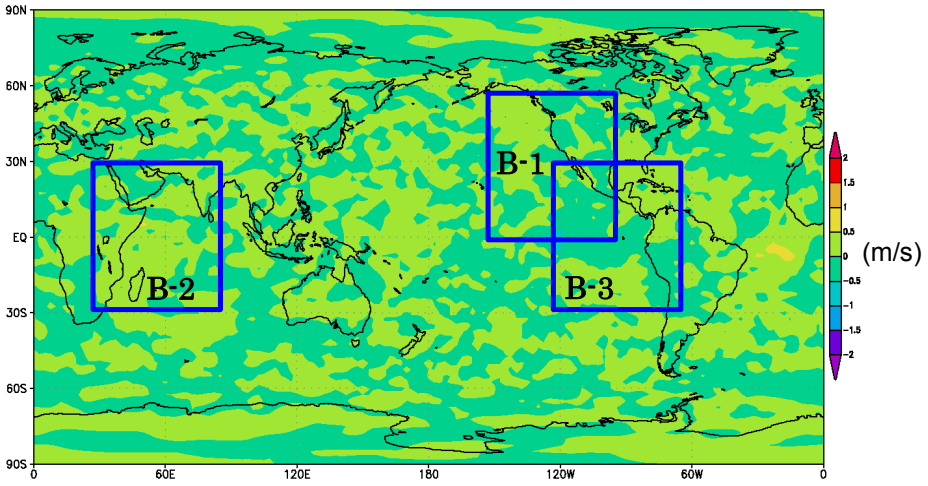

(300hPa)

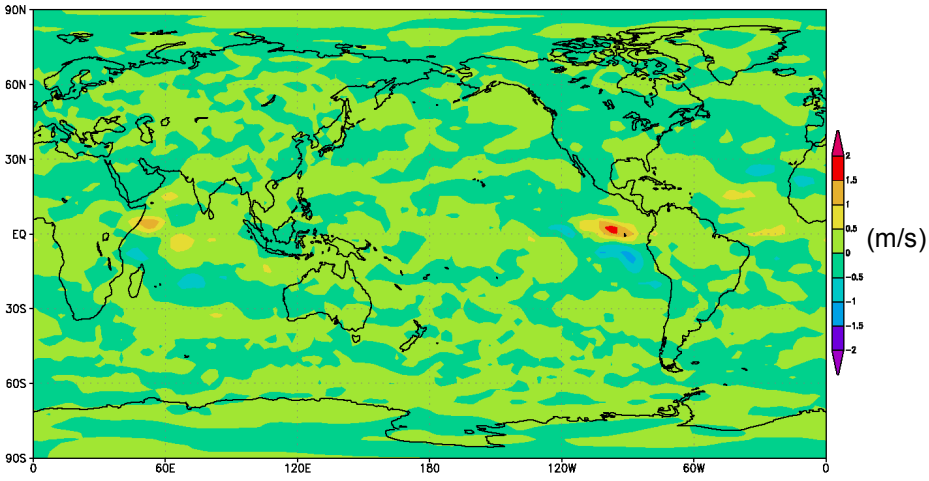

(500hPa)

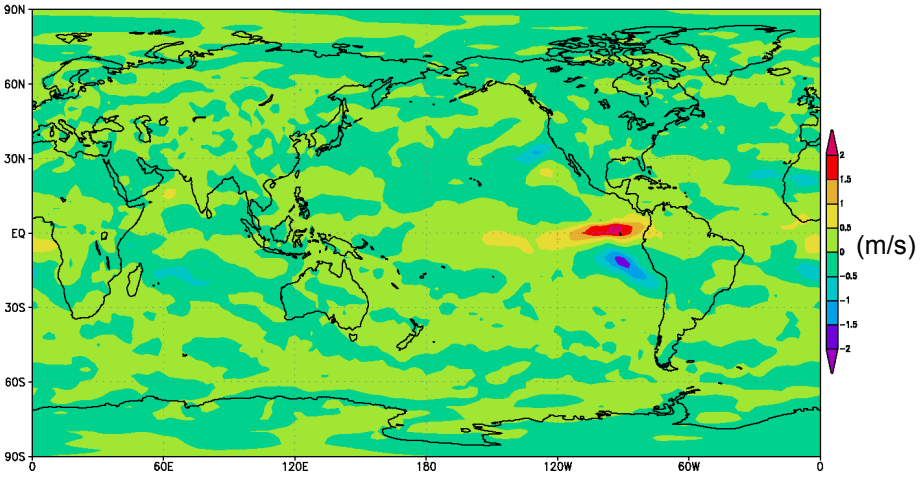

(850hPa)

Figure 11: Difference (CTRL-TEST2) of zonal wind analysis at 300, 500 and 850hPa.

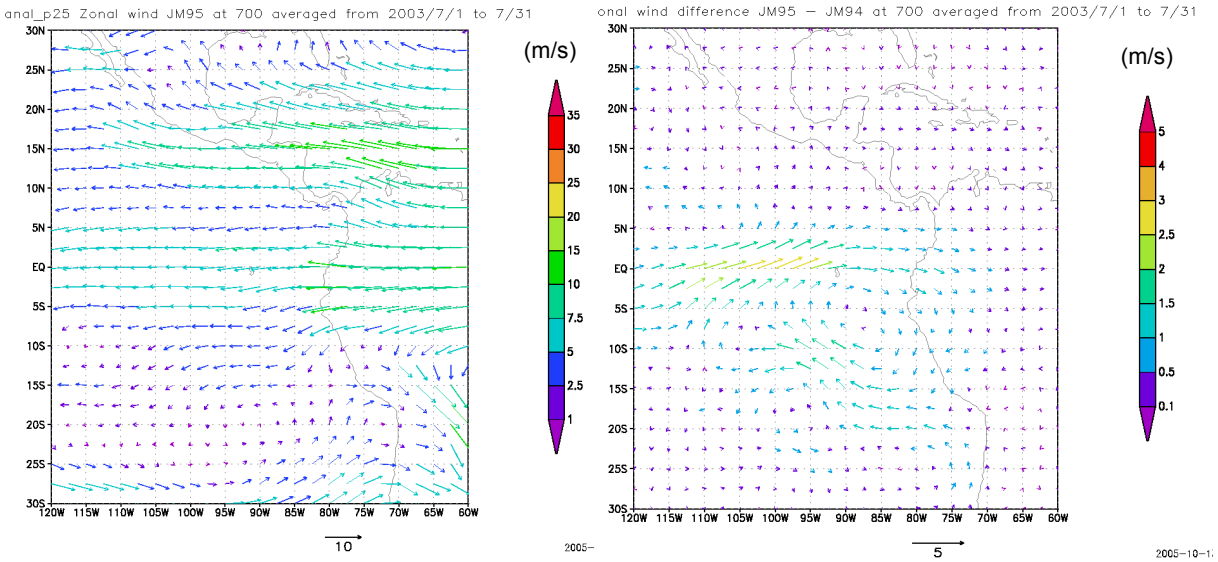

Figure 12-1: Monthly averaged analysis wind at 700hPa of CTRL (Left) and difference of analysis wind at 700hPa between CTRL and TEST2 (Right) for region B-1.

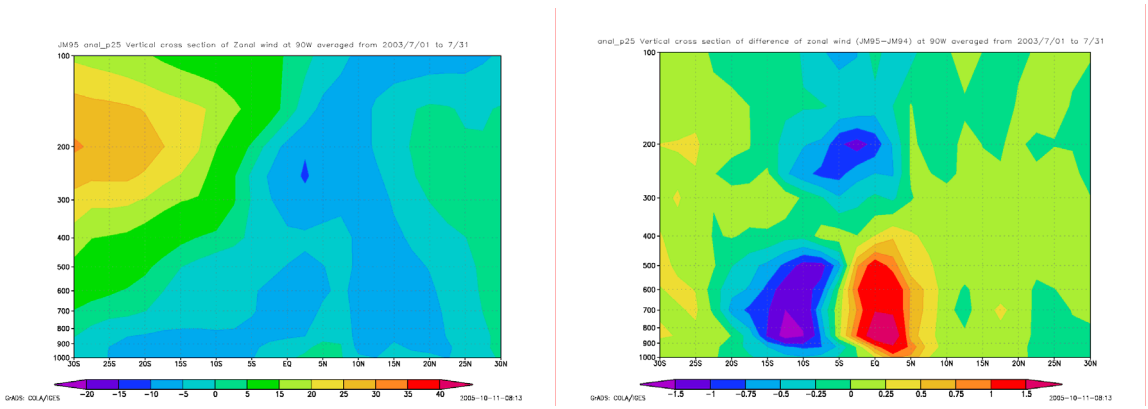

Figure 12-2: Longitudinal vertical cross-sections of zonal wind (m/s) at 90W (for region B-1). Left: Monthly averaged analysis of CTRL, Right: Difference of analysis (CTRL – TEST2).

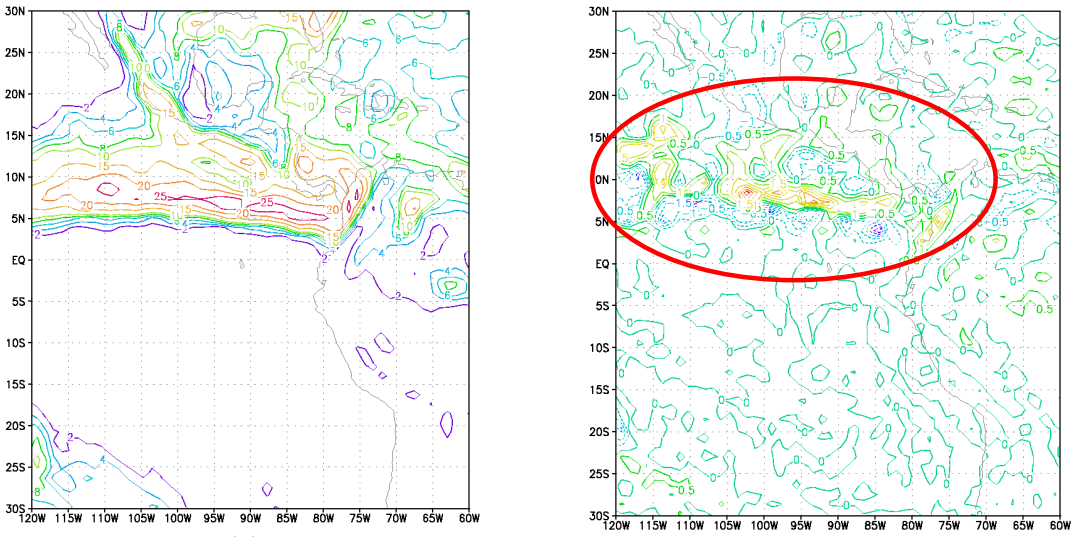

(a) (b)

Figure 12-3: (a) Monthly averaged precipitation rate (mm/hour) of CTRL, and (b) Difference between CTRL and TEST2 for Region B-1.

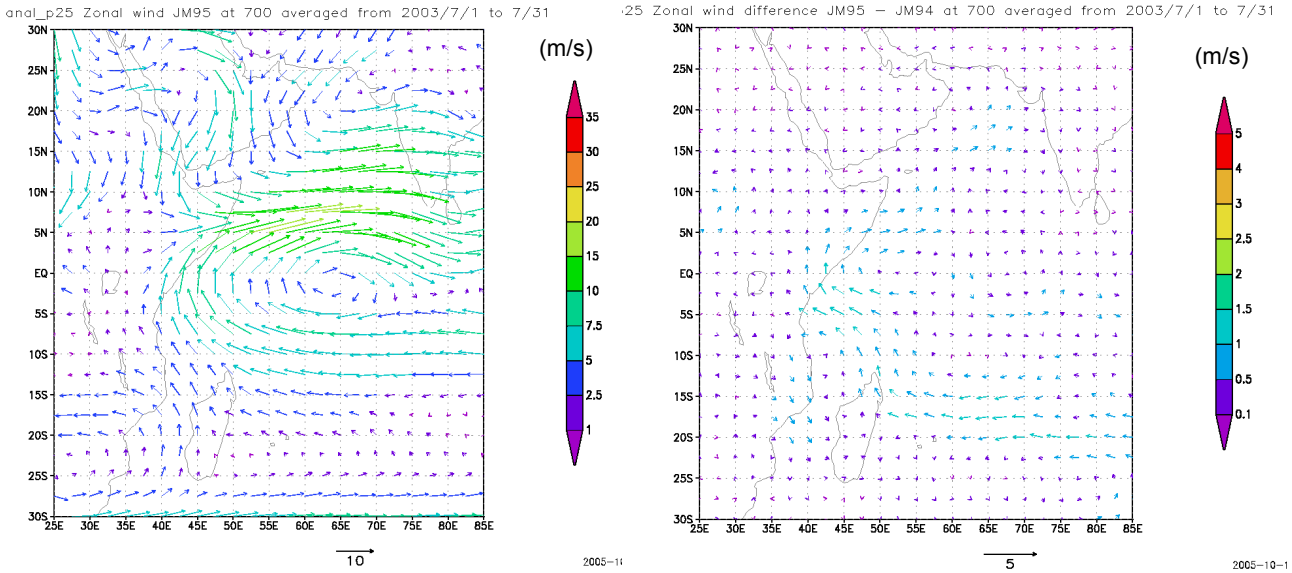

Figure 13-1: Monthly averaged analysis wind at 700hPa of CTRL (Left) and difference of analysis wind at 700hPa between CTRL and TEST2 (Right) for region B-2.

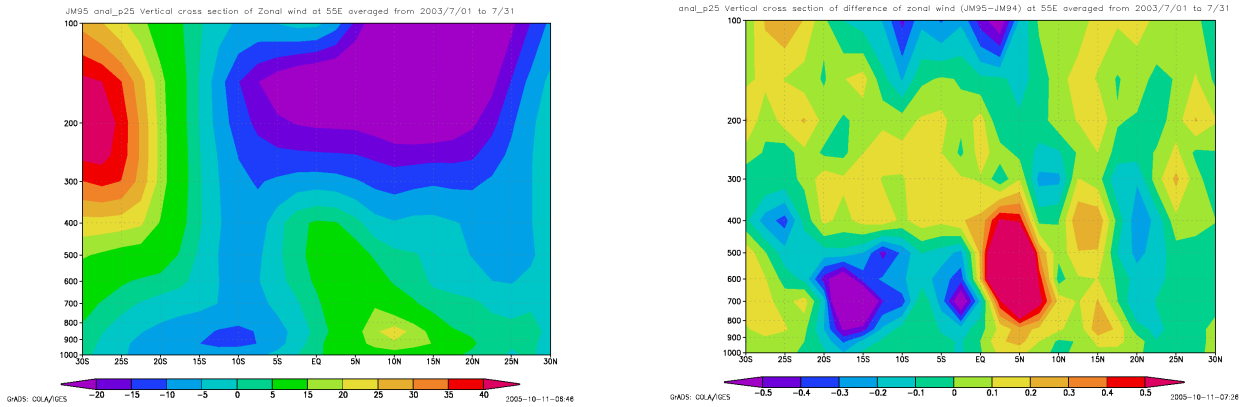

Figure 13-2: Longitudinal vertical cross-sections of zonal wind (m/s) at 55E (for region B-2).
Left: Monthly averaged analysis of CTRL, Right: Difference of analysis (CTRL – TEST2).

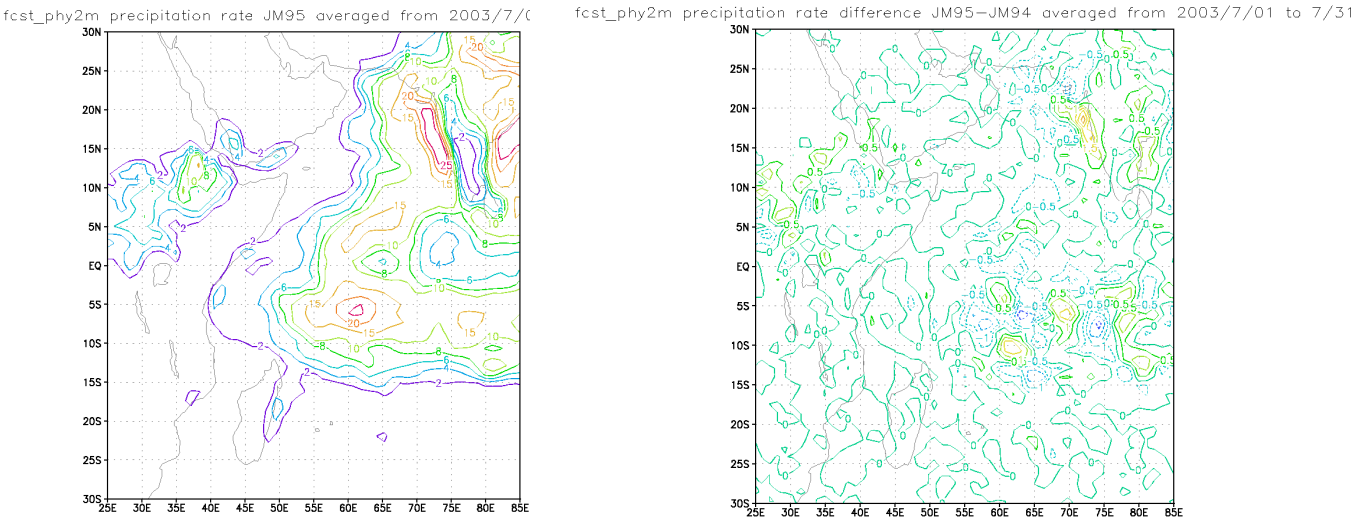

(a) (b)

Figure 13-3: (a) Monthly averaged precipitation rate (mm/hour) of CTRL, and (b) Difference between CTRL and TEST2 in region B-2.

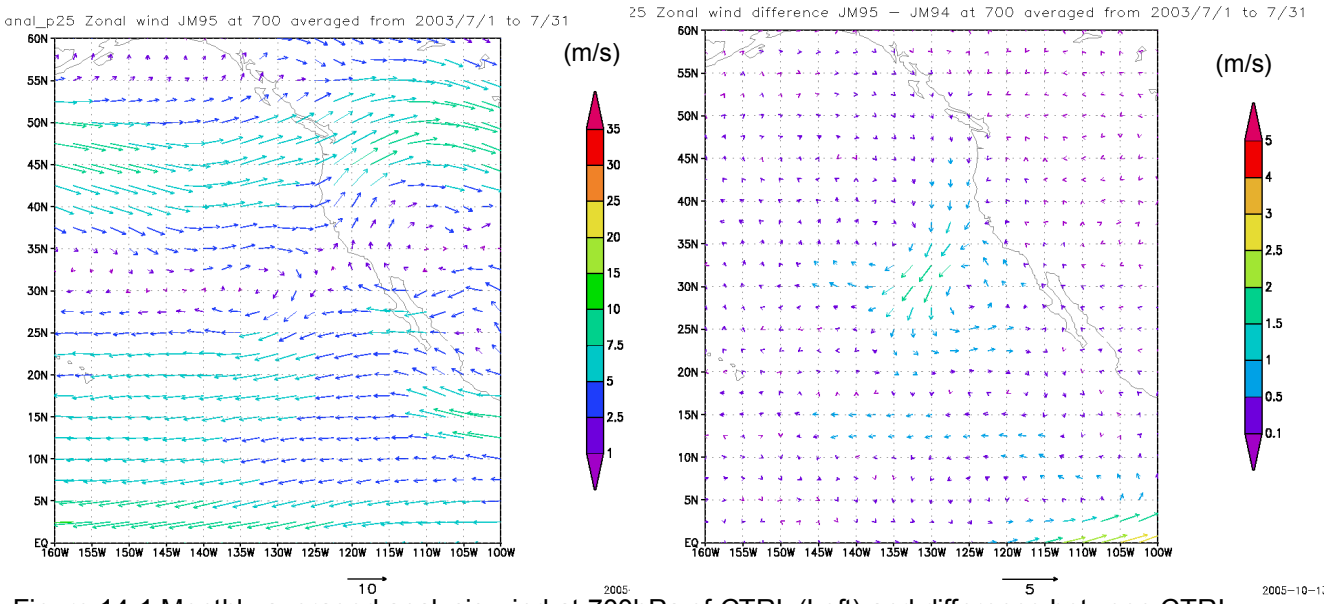

Figure 14-1 Monthly averaged analysis wind at 700hPa of CTRL (Left) and difference between CTRL and TEST2 (Right) for region B-3.

(a)

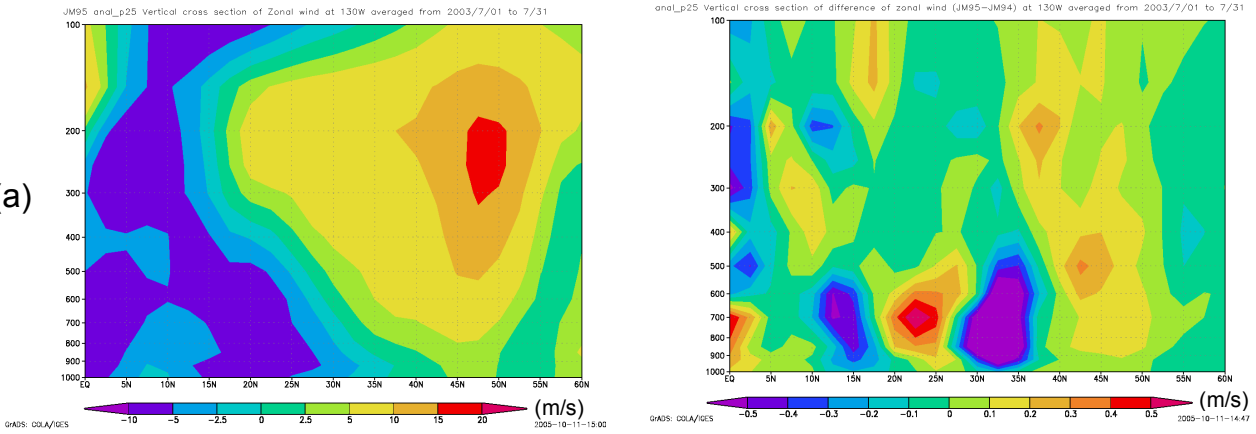

(b)

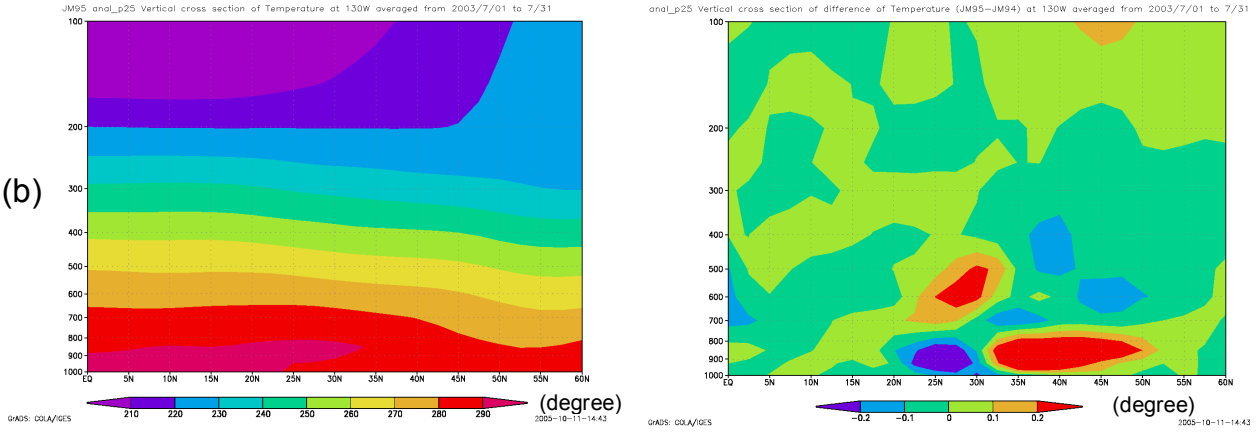

Figure 14-2: Longitudinal vertical cross-sections of each physical value at 130W (for region B-3). Left: Monthly averaged analysis of CTRL, Right: Difference of analysis between CTRL and TEST2. (a) Zonal wind, (b) Temperature.

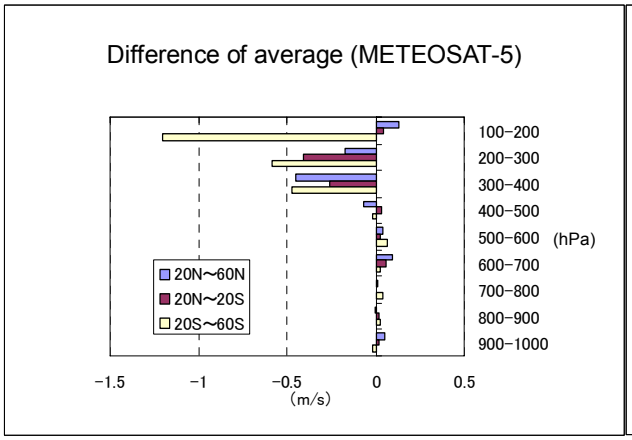

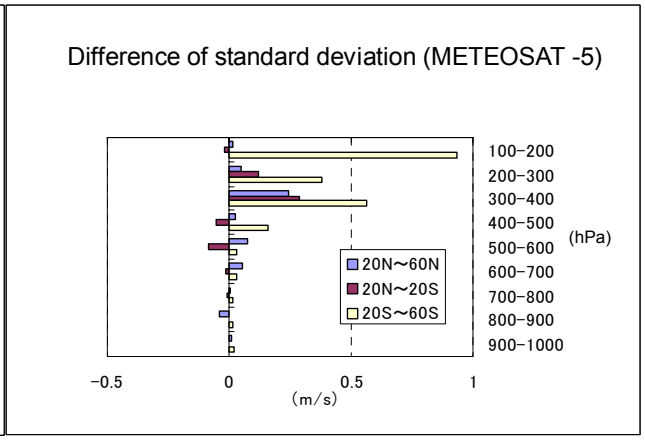

(a)

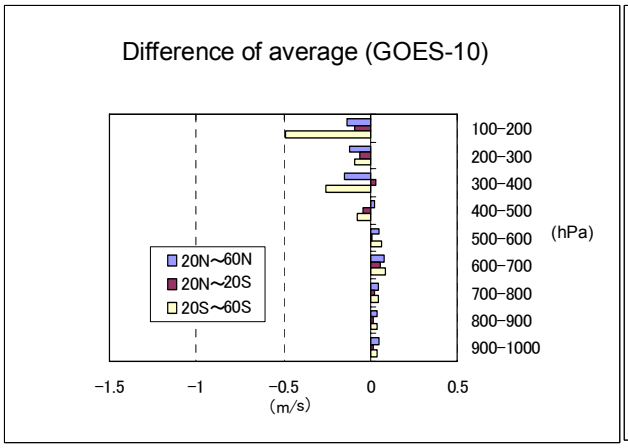

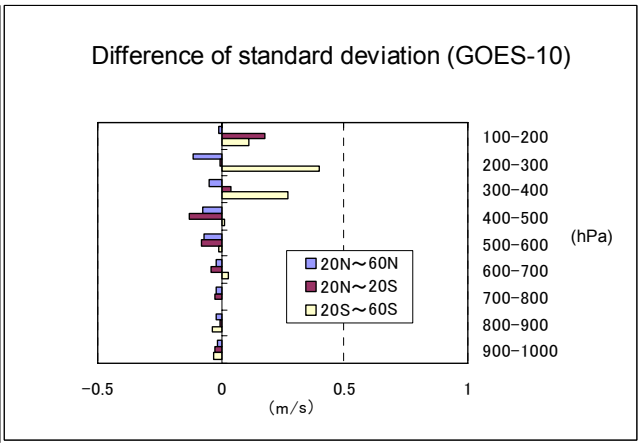

(b)

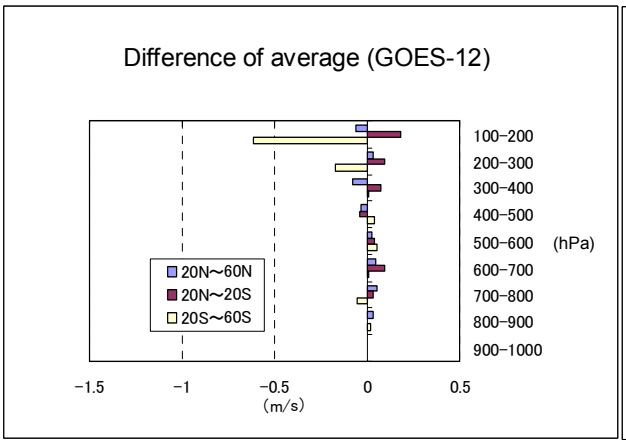

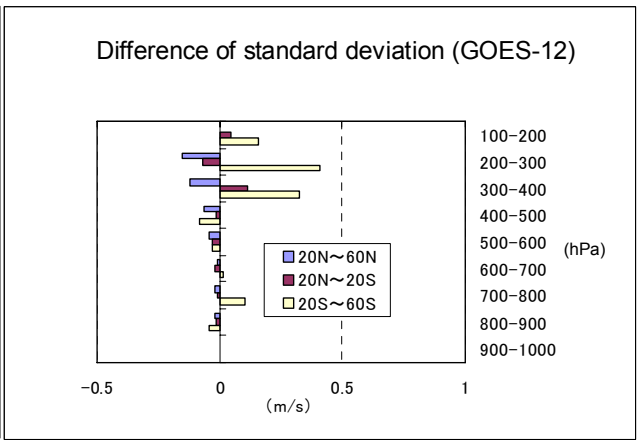

(c)

Figure 15-1: Differences of average (Left) and standard deviation (Right) of Increment of Zonal wind between CTRL and TEST1, which are monthly averaged for each satellite, region and level.
(a) METEOSAT-5, (b) GOES-10, (c) GOES-12.

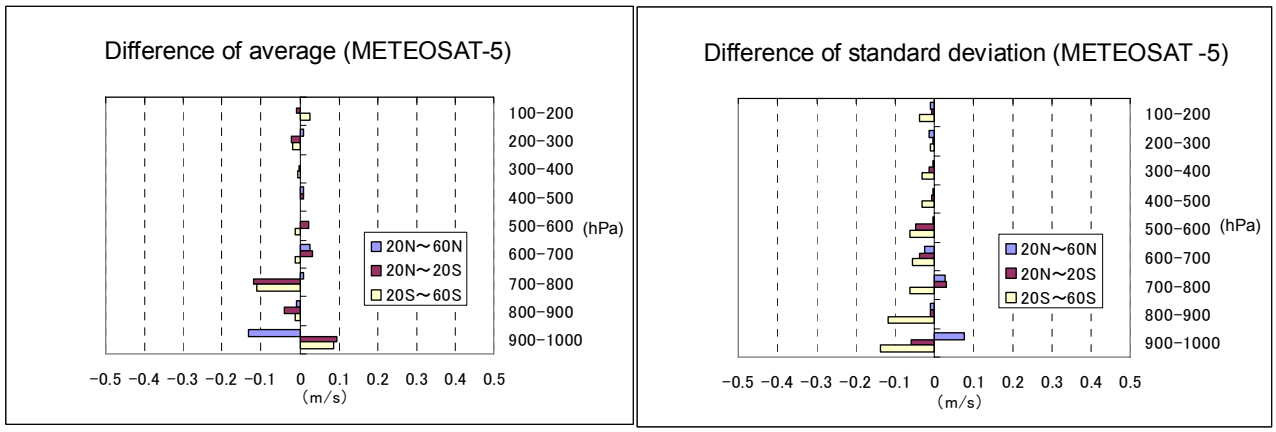

(a)

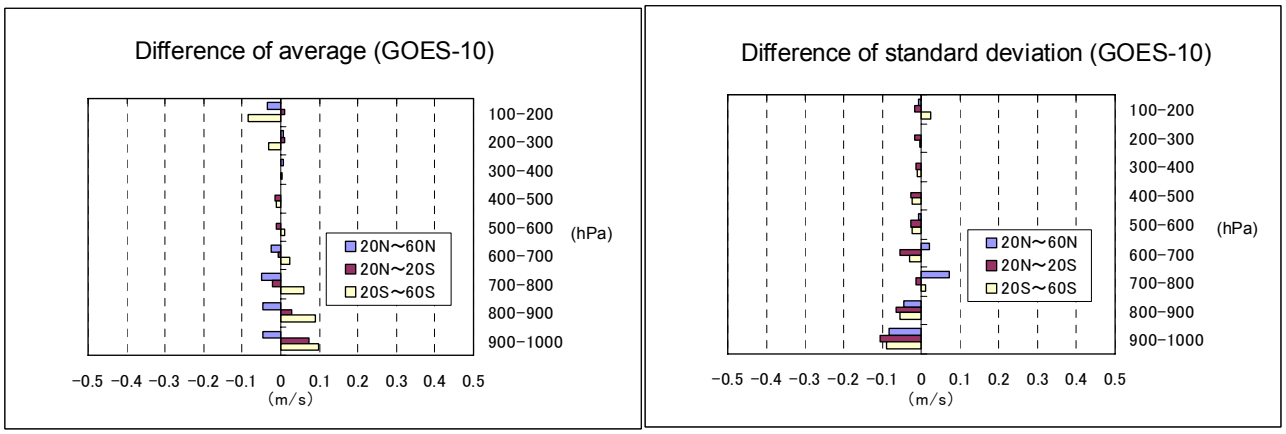

(b)

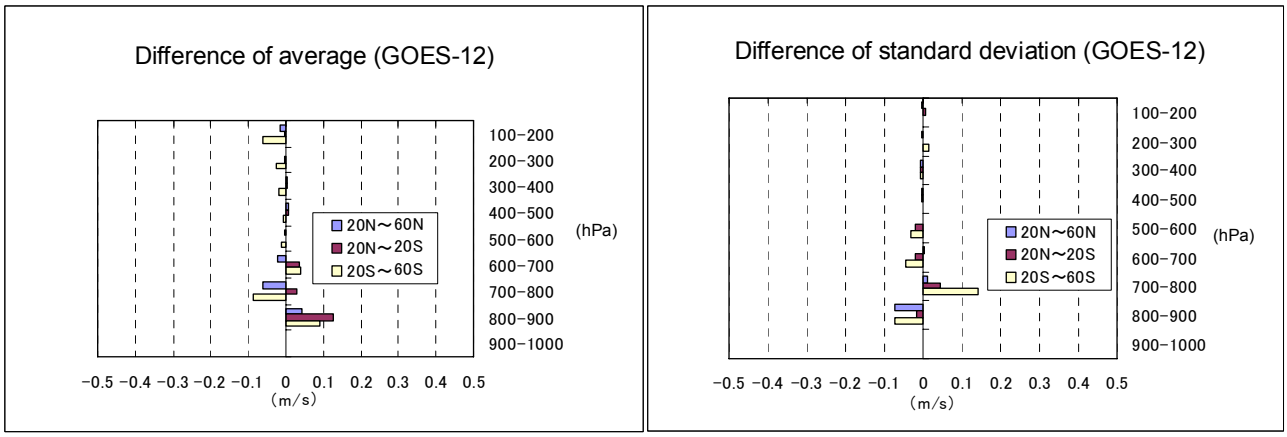

(c)

Figure 15-2: Differences of average (Left) and standard deviation (Right) of Increment (analysis – first-guess) of Zonal wind between CTRL and TEST2, which are monthly averaged for each satellite, region and level. (a) METEOSAT -5, (b) GOES-10, (c) GOES-12.

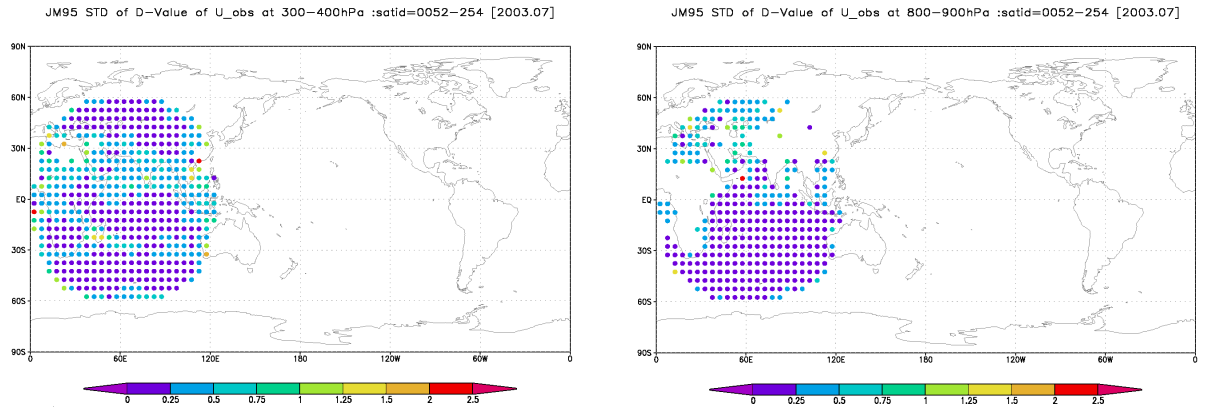

(a)

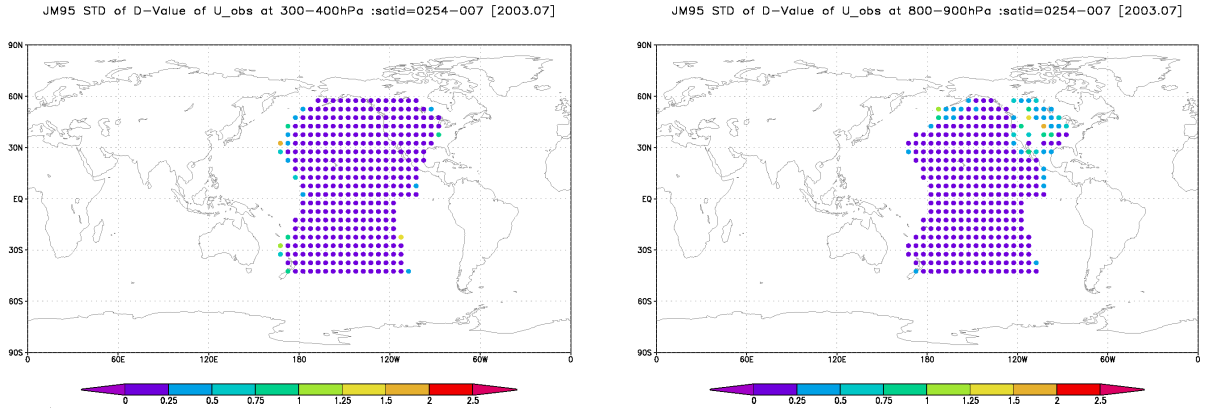

(b)

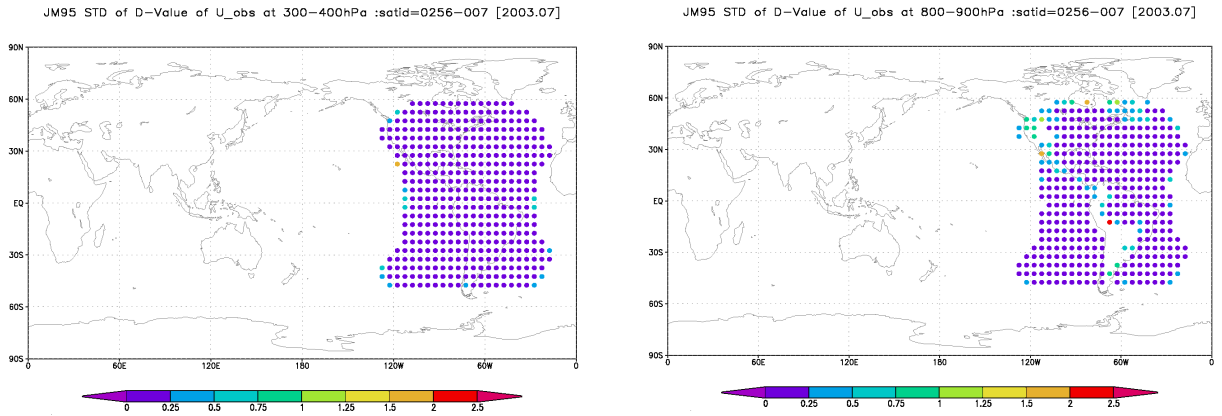

(c)

Figure 16: Monthly Standard Deviation of D-Value (Observation – first-guess) of Zonal Wind of CTRL at 400-300hPa (Left) and 900-800hPa (Right). (a) METEOSAT -5, (b)GOES-10, (c)GOES-12.